

Finite-Element Analysis of Tapered Steel and Fiber-Reinforced Plastic Bridge Camera Poles

Jiwon Jung¹; Ali Abolmaali, M.ASCE²; and Yeol Choi³

Abstract: This paper presents experimental and finite element investigations of the load-deformation behavior of tapered steel and fiber-reinforced plastic (FRP) bridge camera poles subjected to cantilever bending type loading. Three full-scale experimental tests are conducted on one tapered octagonal steel cross section and two FRP circular cross-section poles to identify their load deformation characteristics. Three-dimensional isoparametric finite-element models of the poles are developed by considering the nonlinear coupling behavior between material, contact, and geometric effects. The elastoplastic solid elements with eight nodes are employed for the effective three-dimensional finite-element modeling and analysis. A surface-to-surface contact algorithm is used to simulate the interaction between contact surfaces. An energy-based convergence criterion is adopted to obtain the converged coupled nonlinear solutions. The obtained load-deformation results from finite-element analyses are compared with those of the experiments. The behavior of the finite-element models is examined by observing the effects of individual geometric variables on the load-deformation characteristics of the poles.

DOI: 10.1061/(ASCE)1084-0702(2006)11:5(611)

CE Database subject headings: Finite element method; Steel; Fiber reinforced plastics; Poles; Traffic surveillance.

Introduction

Closed-circuit television (CCTV) cameras and their supporting poles, which are commonly installed on bridges and interstate highways, are one of the key parts an intelligent transportation system. The CCTV camera systems make it possible for departments of transportation to capture information for viewing in transportation management centers, where this information can be shared with both the public and private sectors to increase the mobility, safety, and efficiency of the transportation system. High stiffness and strength of supporting poles are essential for stabilization of the images transmitted by the CCTV cameras. Wind-induced deflection of each pole is a function of the pole's geometric variables and loading, which vary immensely for different regions and applications. For example, a commonly used tapered pole's height may vary from 6.1 m (20 ft) to 19.8 m (65 ft) depending on the applications, which in turn cause variation of other parameters such as base diameter, top diameter, pole thickness, base plate thickness, and bolt diameter. Also, wind loads vary in different regions and seasons, and the vibrations caused by vehicle traffic effect a pole's deflections and ultimately the images transmitted by the cameras. Thus, the lack of the gen-

eralized equations for stiffness and strength of the CCTV poles as the functions of their geometric variables, which lead to informed pole designs, have been under scrutiny (Abolmaali et al. 2004).

Cameras currently in use are supported by wood, concrete, steel, and recently fiber-reinforced plastic (FRP) poles have gained popularity (Lacoursiere 1999). State departments of transportation, including the Texas Department of Transportation, generally use tapered steel poles most often on or at the vicinity of bridge structures (Abolmaali et al. 2004). The California Department of Transportation has recently installed several FRP poles on bridges at different locations (www.dot.ca.gov).

The objective of this study is to develop 3D finite-element analysis (FEA) models to accurately predict the load-deformation characteristics of steel and FRP poles. The behavior of the models is verified with full-scale experimental tests conducted on both steel and FRP poles. Thus, this study sets up the tools necessary to develop regression equations or mathematical models such as three-parameter models (Richard and Abbott 1975) for both poles.

Tapered steel and FRP poles are selected for this study because they are popular among department of transportation officials and constructors (Ibrahim and Polyzois 1999; Polyzois et al. 1999). The following are in forefront among the advantages of steel poles when compared to conventional concrete and wood poles: high strength, long life, and factory predrilling reduced maintenance costs. Some characteristics of FRP poles that are superior to those of steel poles are their light weight, high strength-to-weight ratio, and stiffness tailored capability (Lin 1995).

A few investigations on steel and FRP poles have been performed to predict their load-deflection behavior. Polyzois et al. (1999;1998) conducted experimental and analytical studies to identify the critical buckling load of FRP poles with hollow circular cross-sections. Studies conducted by Lin (1995) concluded that the behavior of FRP poles is dependent on material configurations, geometries, and loading and boundary conditions. Ibrahim and Polyzois (1999) performed nonlinear analyses to determine the behavior of tapered FRP poles by means of changing fiber angles and wall thicknesses. Dicleli (1997) concluded that,

¹Ph.D. Candidate, Dept. of Civil and Environmental Engineering, Univ. of Texas at Arlington, Arlington, TX 76019. E-mail: jxj8144@uta.edu

²Assistant Professor, Dept. of Civil and Environmental Engineering, Univ. of Texas at Arlington, Arlington, TX 76019 (corresponding author). E-mail: abolmaali@ce.uta.edu

³Assistant Professor, School of Architectural Engineering, Kyungpook National Univ., 1370 Sankyuk-dong, Buk-gu, Daegu, 702-701, Korea.

Note. Discussion open until February 1, 2007. Separate discussions must be submitted for individual papers. To extend the closing date by one month, a written request must be filed with the ASCE Managing Editor. The manuscript for this paper was submitted for review and possible publication on April 14, 2005; approved on September 27, 2005. This paper is part of the *Journal of Bridge Engineering*, Vol. 11, No. 5, September 1, 2006. ©ASCE, ISSN 1084-0702/2006/5-611-617/\$25.00.

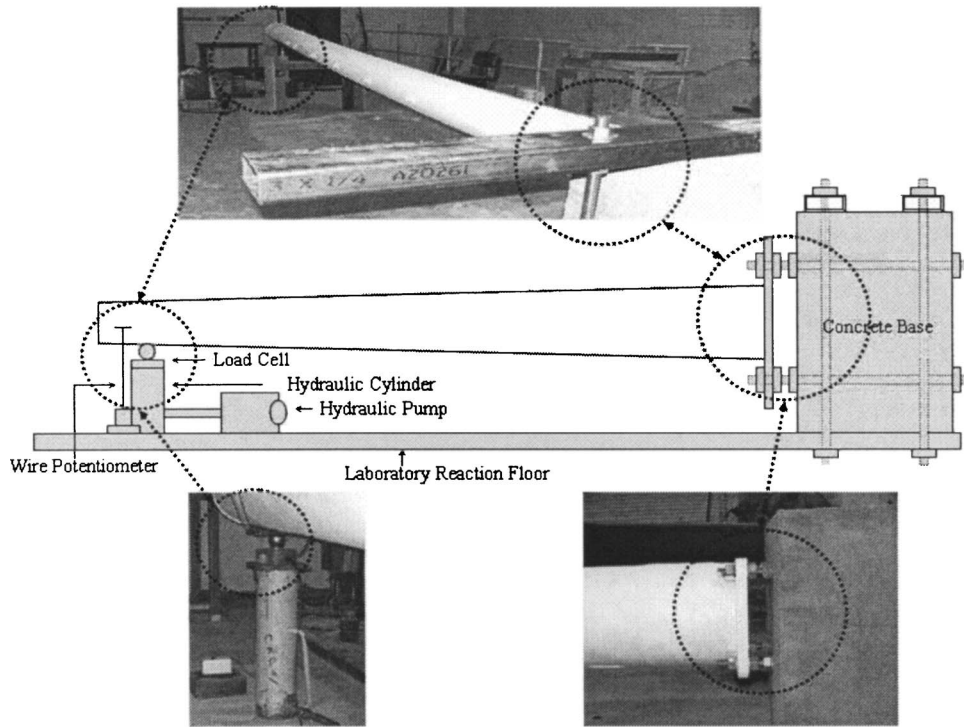


Fig. 1. Typical configuration of test setups

for pole structures with cross-sections made of regular polygons, the flexural capacity increases as the number of sides of the polygon increases when the cross-section's circumference and thickness remain constant. Fu and Boulos (1996) used FEA-based investigation to propose design equations for the base plates of signal poles by considering stress concentration as a failure mode.

Limited literature exists on the experimental and FEA of tapered poles. However, the literature is rich for experimental testing and FEA of beam-to-column steel connection assembly, which is similar in geometry and behavior to pole assembly. For example, in testing for the moment-rotation behavior of steel connection, a beam is welded to an end-plate (or angles), which is bolted to column flange. This is similar to the pole assembly in which a pole is welded to an end plate that is bolted to the concrete base. Thus, among related literature reported on steel connections, researchers such as Krishnamurthy (1978) and Kukreti et al. (1990) developed detailed finite element models for large capacity extended end-plate connections and compared their analysis results with those of experiments. Yorgun et al. (2004) used FEA to develop a three-dimensional model of the connection that included material nonlinearity and strain hardening for end-

plate and bolt components. The adequacy of their analytical model was verified through comparisons with reference tests. Bahaari and Sherbourne (2000) investigated nonlinear behavior of bolted connections considering the plasticity of the material and changes in the contact area. A325 slip critical bolts were used to assemble the connections. Wanzek and Gebbeken (1999) and Citipitioglu et al. (2002) emphasized the importance of through-thickness deformation in the analysis of steel end-plate connections by using three layers of elements through the thickness of the end plate. The effects of friction and slip on the response of connections were also considered. Chutima and Blackie (1996) investigated the effect of pitch distance, row spacing, and bolt

Table 1. Geometric Variables of the Steel and FRP Connection Assembly

Concrete	Steel/FRP	914 mm × 914 mm × 1219
Bolt	Steel	13 mm (1/2 in.)
	FRP	29 mm (1 1/8 in.)
Bolt	Steel	14 mm (1/2 + 1/16 in.)
	FRP	30 mm (1 1/8 + 1/16 in.)
Gap	Steel	19 mm (3/4 in.)
	FRP	64 mm (2 1/2 in.)
Anchor	Steel	13 mm (1/2 in.)
Diameter	FRP	29 mm (1 1/2 in.)

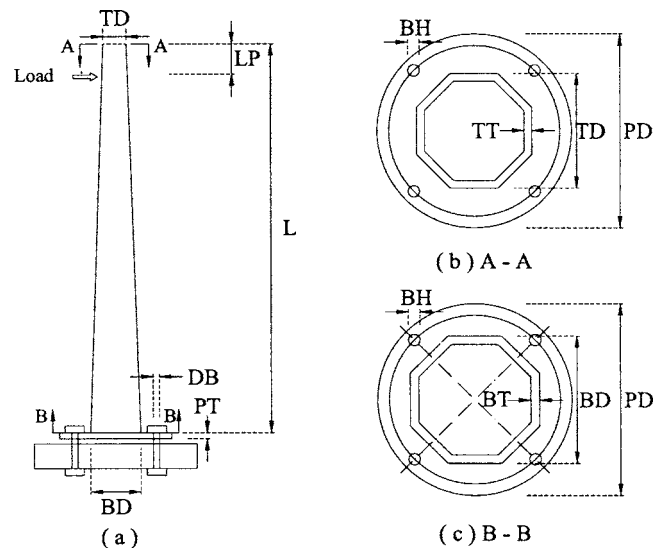


Fig. 2. Dimensions of steel pole tested

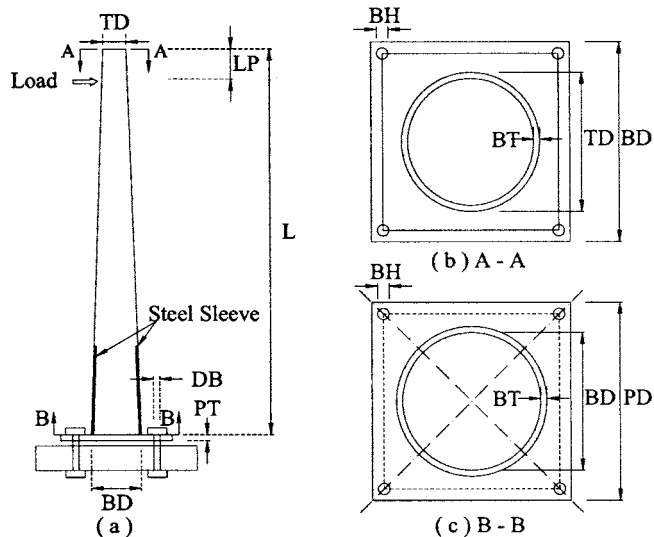


Fig. 3. Dimensions of FRP pole tested

diameter on composite joints. Stallings and Hwang (1992) presented a simple pretensioning model in the FEA of bolted connections by using temperature changes for the bolts modeled with rod elements. Kulak and Birkemoe (1993) conducted field studies on bolt pretension. This study showed that actual pretensions were 35% greater than specified minimum pretensions. Therefore, bolt pretension would be at least 70% of the ultimate tensile strength of the bolt.

Experimental Program

The test setup consisted of a steel or FRP pole and concrete base assembly, which were complemented with a hydraulic-load cylinder, hydraulic pump, position transducer, and digital data acquisition system as shown in Fig. 1. The concrete base with a 28-day compressive strength of 24 MPa (3480 psi), a 914 mm \times 914 mm (3 ft \times 3 ft) cross-section, and a 1.22 m (4 ft) length was bolted to the laboratory floor by four 13 mm (1/2 in.) or 29 mm (1 1/2 in.) diameter threaded rods. The steel and FRP poles were welded to steel end plates and bolted to the concrete base. The gap between the base plate and the concrete base was 19 mm (3/4 in.) and 64 mm (2 1/2 in.) for steel and FRP test

Table 2. Geometry of Test Specimens

Specimen	Steel mm (in.)	FRP1 mm (in.)	FRP2 mm (in.)
L	6096 (240)	6096 (240)	7620 (300)
LP	460 (18)	460 (18)	570 (22)
LS	0	610 (24)	610 (24)
TD	84 (3.3)	259 (10.2)	244 (9.6)
BD	132 (5.2)	305 (12)	305 (12)
DB	13 (0.5)	29 (1.125)	29 (1.125)
BH	14 (0.55)	30 (1.18)	30 (1.18)
TT	3 (0.125)	10 (0.375)	10 (0.375)
BT	3 (0.125)	11.4 (0.45)	12 (0.475)
PT	10.7 (0.42)	32 (1.25)	32 (1.25)
PD	221 (8.7)	346 (13.6)	346 (13.6)

Table 3. Material Properties of the Steel Pole

Material Properties	Plate (A36)	Bolt (A325)
E	206 GPa (30 Msi)	206 GPa (30 Msi)
F_y	248 MPa (36 ksi)	634 MPa (92 ksi)
ν	0.29	0.29
E_t	2 GPa (300 ksi)	2 GPa (300 ksi)
μ	0.2	0.2

specimens, respectively. Table 1 summarizes the dimensions of the geometric variables of the steel and FRP poles' connection assembly.

The configuration and dimensions of the specimens tested are shown Figs. 2 and 3 for steel and FRP poles, respectively, and their numerical values are presented in Table 2. The poles were designed based on the Standards and Specifications of the Texas Department of Transportation and the California Department of Transportation for steel and FRP poles, respectively. As shown, the length of the steel pole was 6.1 m (20 ft), and its octagonal cross section was welded to the end plate, which was bolted to a concrete base using four 13 mm (.5 in.) threaded rods. The wall thickness of the steel pole was 3.2 mm (.125 in.), and its outer base and top diameters were 132 mm (5.2 in.) and 84 mm (3.3 in.), respectively. The base plate was circular with a 221 mm (8.7 in.) diameter, and its thickness was 10.7 mm (0.42 in.).

Table 2 also shows that the heights of the FRP poles were 6.1 m (20 ft) and 7.6 m (25 ft). The FRP poles were fabricated by a filament winding wet process, which was made of vinyl ester reinforced with E-glass fibers. The poles were composed of 30% unsaturated polyester blend (resin) and 70% standard electrical glass (fiber), also known as E-glass by weight. A 610 mm (24 in.) long and 6 mm (.25 in.) thick steel sleeve was inserted in the pole and was welded to the steel base plate (Fig. 3), which was bolted to the concrete base by 29 mm (1.5 in.) A325 threaded rods. The gap distance between the end plate and concrete base was 64 mm (2 1/2 in.) as shown in Fig. 3 and Table 1. This gap allowed for the placement of the leveling nuts between the end plate and concrete base to facilitate the adjustments of the pole during installation (Fig. 1). The thickness of the FRP poles was varied such that their cross-sectional area remained constant to meet manufacturer's standards and specifications, which complied with certain FRP poles used by the California Department of

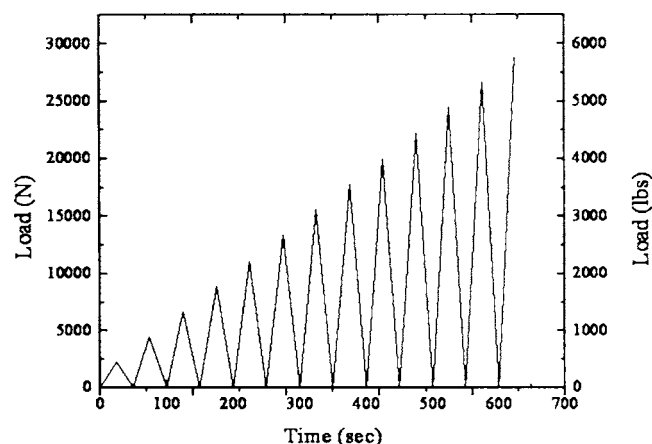


Fig. 4. Loading history

Table 4. Material Properties of the FRP Poles

Material properties	E_x GPa (Msi)	σ_x Mpa (ksi)	G GPa (Msi)	ρ kg/m ³ (lb/in. ³)	μ	w_f (%)	v_f (%)	δ_u (%)
E-glass	72.4 (10.5)	3,448 (500)	30 (4.4)	2,540 (0.09)	0.2	70	50	4.8
Vinylester	4.14 (0.6)	90 (13)	1.38 (0.2)	1,090 (0.039)	0.2	30	50	4.2

Transportation on and at the vicinity of bridges. For example, the thickness of the first FRP test specimen was varied from 10 mm (.375 in.) at the bottom to 11 mm (0.45 in.) at the top (Table 2). Finally, the material properties of steel and FRP poles are presented in Tables 3 and 4, respectively.

The load was applied incrementally by the Enerpac P-80 hydraulic pump and Enerpac RC 5013 load cylinder to the pole in the vertical direction (Fig. 1). The load cylinder had a 490 kN (110 kips) load capacity and exerted a perpendicular load at 460 mm (18 in.) below the tip of the pole. A load cell was mounted on the hydraulic cylinder; this measured the applied load and transferred the information to the precise digital controller for storing. The deflection of the pole was measured by using a position transducer, which was attached at 460 mm (18 in.) from the pole's tip. Fig. 4 shows a typical incremental loading history, which was employed to apply the load in increments of approximately 20 N (4.5 lb) per s. At the end of each load increment the specimens were unloaded to zero to capture nonlinear behavior caused by material and/or geometry.

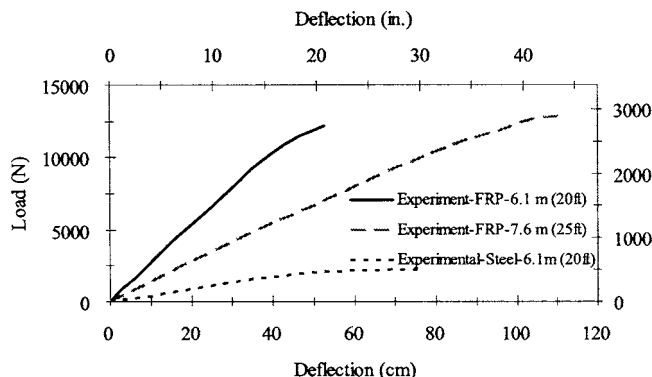
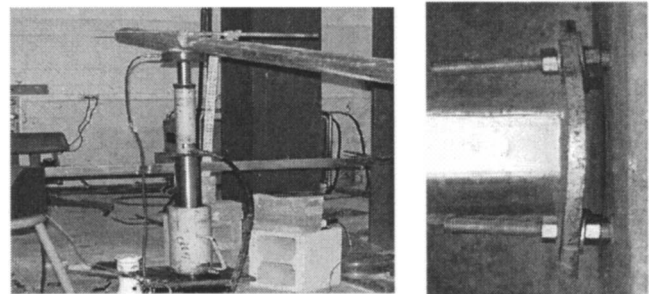
The experimentally obtained load-deflection plots of the steel and FRP poles are presented in Fig. 5, which shows that the FRP pole with 7.6 m (25 ft) in length is more flexible than the one with 6.1 m (20 ft) in length. Also, this figure shows that the load deflection for the steel pole is the most flexible among the three because the steel pole's thickness was considerably less than that of the FRP poles. For example, steel pole's thickness at the top is about 33% of that of the FRP. The testing was stopped for steel poles because of their excessive tip deflection. Also, yielding at steel poles' base plate was observed and was accompanied by permanent elongation of the bolts in the tension region (Fig. 6). However, no yielding was detected throughout the pole's length in the steel test poles. The FRP poles also experienced excessive tip deflection before testing was terminated. Permanent bolt elongation was also observed in the tension region; however, the end plate did not yield because it was relatively thick. In both tests for the FRP poles, initial superficial cracks formed at an early stage of loading (i.e., 2,670 N [600 lbs]), as shown in Fig. 7. Also at early stages of loading and unloading delamination of the FRP fiber was noticed through the sounds transmitted by the test speci-

mens, which continued throughout the testing. However, the initial cracks and fiber delaminations did not cause any degradation in the stiffness of the FRP test poles (Fig. 5).

Finite Element Model

Three-dimensional nonlinear FEA models for the steel and FRP poles were generated using the FEA software package ANSYS. Since a plane of symmetry exists along a section through the longitudinal axis of the pole, base plate, and concrete base, one-half of the pole and its connection assembly were modeled for the analyses as shown in Fig. 8. Thus, symmetric boundary conditions were defined for the nodes along the plane of symmetry. Plastic quadrilateral eight-node solid elements, SOLID45 in ANSYS, were used to model steel pole, steel plate, bolt head and nut, and concrete base. This element has three translational degrees of freedom at each node, with the capability to accept algorithms for material, contact, and geometric nonlinearities.

The bolt model was constructed so that it was divided into bolt shank, head, and nut elements in order to consider their individual effects on the pole behavior. In the early finite element studies of bolted connections such as those by Choi and Chung (1996), pretension effects in the bolts caused by the tightening of each bolt were simulated by applying compressive forces equivalent to proof load (70% of bolt's ultimate tensile strength) to the end plate at the location of bolt head and nut. This made it difficult to monitor the variation of the bolt force during the analysis. Thus, ANSYS's bolt pretension element, a 3D line element that connects the two imaginary parts of the bolt shank, was used. The pretension element, as shown in Fig. 8(d) contains nodes 'I' and 'J', located at an arbitrary section through the bolt shank length and connected with a link element. The aforementioned section is selected arbitrarily to comply with different mesh configurations. Node K is the pretension node with one degree of freedom, u_x , with the actual line of action in the pretension load direction. The underlying bolt elements can be solid, shells, or beam elements of any order of polynomial. When the pretension is applied on the node K, the link element joining nodes I and J will be in tension. This in turn pulls the two imaginary sections of the bolt toward each other to compress the connecting surfaces. During the pre-

**Fig. 5.** Experimental results**Fig. 6.** Typical steel specimen at failure

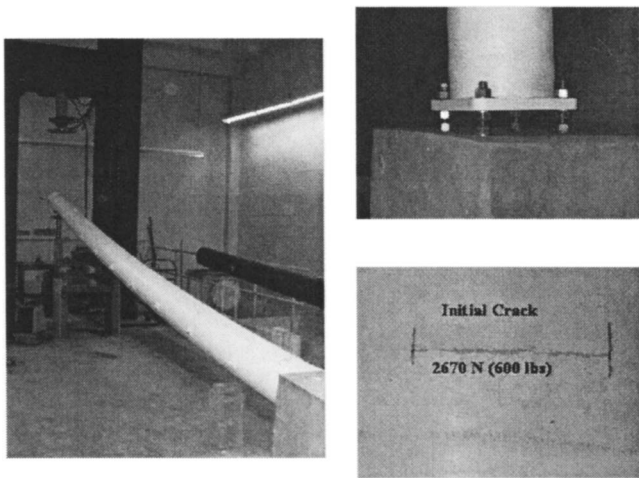


Fig. 7. Typical FRP specimen at failure

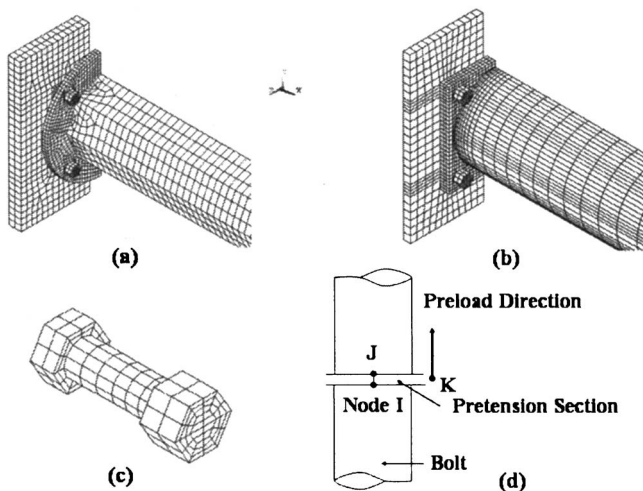


Fig. 8. Finite element model: (a) typical steel pole; (b) typical FRP pole; (c) bolt; and (d) pretension element used

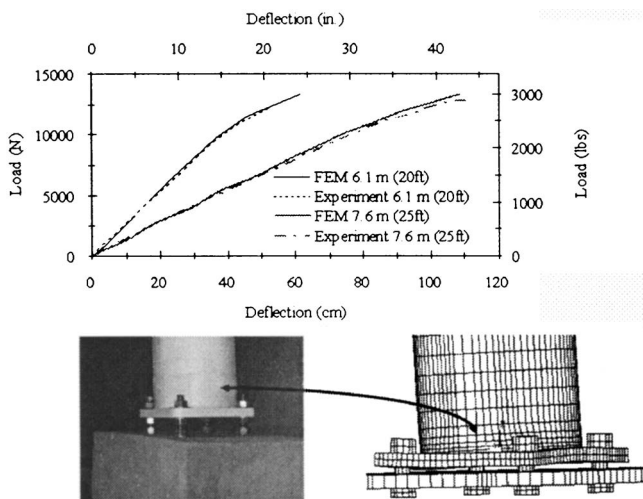


Fig. 9. Comparison of load-deflection relation in FRP poles between experimental and finite element results

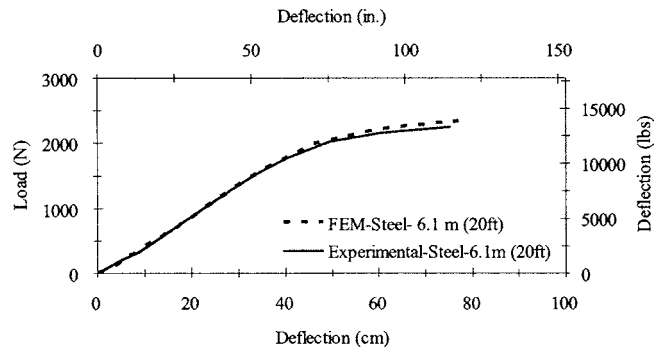


Fig. 10. Comparison of load-deflection relation in steel poles between experimental and finite element results

tensioning of a physical bolt, turning of the nut reduces the unstretched grip length of the bolt, thereby inducing pretension. When the desired pretension is achieved and the wrench is removed, the new unstretched grip length becomes locked. The pretension element used applies the same procedure during the loading in the same sequence: First, the specified pretension load is applied incrementally to capture contact nonlinearity and possible nonlinearities induced by material yielding. At this point in the analysis, the pretension section displacement is locked for the pretensioned bolt. Once all bolts are pretensioned and locked, external load is applied incrementally to capture nonlinearities caused by material, geometry, and contact. Since the monotonic convergence of nonlinear problems by finite element method in general is problem dependent and not guaranteed, an improved convergence was obtained by employing energy-based convergence criteria.

A contact model with a small sliding option was applied between the contact pair surfaces of all connecting elements, including bolt shanks and bolt holes and bolt head/nut and connecting components. Surface-to-surface and flexible-to-flexible contact type was used in the FEA algorithm because contacts between surfaces were deformable finite elements (Kishi et al. 2001). All components including bolts were completely independent from each other as assemblages in real connection. A coefficient of friction of 0.2 was used as observed by Yorgun et al. (2004).

Finally, the material behavior for each pole, end plate, and bolt was described by bilinear stress-strain curves as defined in Tables 3 and 4 for steel and FRP poles, respectively. The initial slope of the curve was taken as the elastic modulus, E , of the material. After several trials to best calibrate the FEA model with the ex-

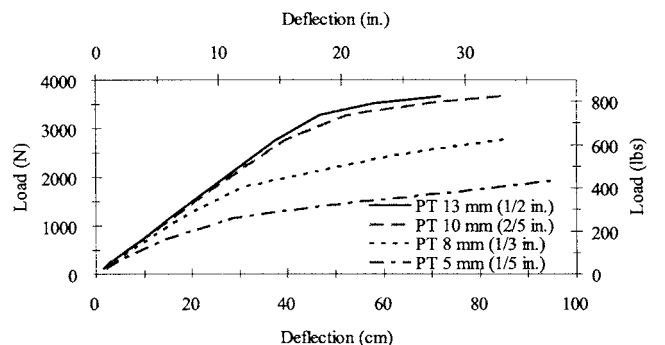


Fig. 11. Effect of variation of base plate thickness on load-deflection characteristics of steel poles

Table 5. Load-Deflection Results for Steel and FRF Poles Tested

Test Specimens	Load N (lbs)		Max. displacement cm (in.)		Error (%)
	Experimental	FEA	Experimental	FEA	
Steel 6.1 m (20 ft)	2,247 (505)	2,332 (524)	75.25 (29.63)	77.18 (30.39)	2.5
FRP 6.1 m (20 ft)	12,200 (2742)	12,485 (2806)	52.63 (20.72)	53.28 (20.98)	1.2
FRP 7.6 m (25 ft)	12,856 (2889)	13,350 (3000)	111.02 (43.71)	108.67 (42.78)	2.2

perimental results obtained, the post-yield stiffness identified as tangent modulus E_t was taken as 1% of the initial stiffness ($E_t=0.01E$). Plasticity-based isotropic hardening, which uses the Von Mises yield criterion, was used to obtain the response of the pole in the inelastic region.

Finite Element Results and Validation

The coupled nonlinear analysis algorithm was employed to analyze the steel and FRP test specimens. Figs. 9 and 10 present comparisons of FEA with experimentally obtained load-deflection relationships for steel and FRP poles, respectively. This comparison shows that the FEA predicts the poles' behavior with high degree of accuracy with maximum error of 2.5% for steel poles and 2.2% for FRP poles (Table 5). The authors believe that the accuracy of the FEA model results from the following factors: (1) introduction of the exact values of the geometric parameters of the pole, which included dimensions and shapes of pole's end plate, length, cross-section, bolt head, bolt shank, and bolt nut; (2) detailed and extensive efforts in calibrations for values for modulus of elasticity (E) for FRP and the post-yield stiffness in the model ($E_t=0.01E$); and (3) use of energy-based convergence criteria for the coupled nonlinear problem studied.

A validation-type study was conducted to verify the behavior of the FEA algorithm further and converged mesh for steel and FRP poles by studying the effects of pole's geometric variables on its load-deflection behavior. Figs. 11 and 12 present the FEA-obtained load-deflection graphs for the steel pole by varying the end-plate thickness and pole thickness, respectively. These figures show that as end-plate thickness or pole thickness increases the tip displacement decreases as expected. Similar intuitive load-deflection behavior was observed when all geometric variables of the steel and FRP pole assembly were varied.

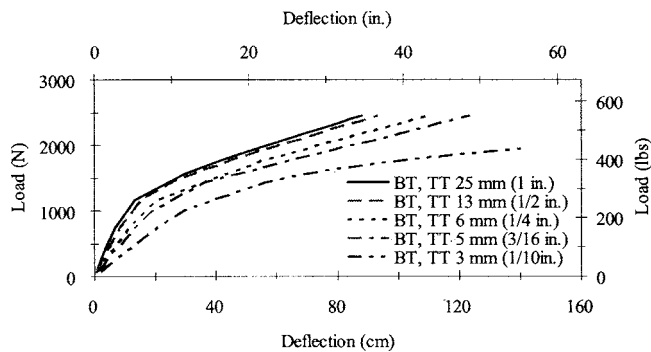


Fig. 12. Effect of variation of wall thickness on load-deflection characteristics of steel poles

Summary and Conclusion

Experimental and finite element method-based studies were conducted on tapered steel and FRP bridge poles to identify their load-deflection behavior. One steel and two FRP poles, each welded to an end plate, which was bolted to a concrete block, were tested in the laboratory. The concrete block was bolted to the laboratory reaction floor by means of threaded rods, which were placed in the forms before casting the concrete. This mimicked the actual field condition in which bridge poles are installed. Each test pole was loaded incrementally, and at the end of each load increment the specimen was unloaded to zero. This allowed any nonlinear behavior induced by material, geometry, or contact to be captured. The applied load was recorded, and the tip displacement was measured using a wire potentiometer, which was placed at the vicinity of the load cell.

The testing was terminated for all the test specimens of steel and FRP poles because of excessive pole tip deflection. For the case of steel pole, end-pole yielding was observed along with permanent bolt elongation in the tension region. At early stages of loading (i.e., 2,750 N [600 lbs]) the initial superficial crack formation was observed in the FRP test specimens and was accompanied with delamination sounds that continued throughout the testing.

3D finite element models of the steel and FRP poles were developed using ANSYS software. Because a plane of symmetry existed along a section through the longitudinal axis of the pole, one-half of the pole and its connection assembly were modeled. The analysis algorithm included nonlinearities caused by material, geometry, and contact with employing an energy-based convergence criterion. The results obtained from the FEA for the load-deflection curves were compared with those of the experiments, which showed that the FEA predicted the poles' behavior closely with maximum errors of 2.5% and 2.2% for the steel and FRP poles, respectively.

To further verify the FEA analysis, the poles' geometric variables were varied, one at the time. The FEA obtained load-deflection results showed the expected and intuitive results.

Acknowledgments

The financial support of the Texas Department of Transportation is gratefully acknowledged. The authors wish to express appreciations to JEM Engineering of Tulsa, Oklahoma, for providing the steel poles and Shakespeare Composite of Newberry, South Carolina, for providing the composite poles test specimens.

Notation

BD = diameter at bottom of pole;
 BH = diameter of bolt hole;
 BT = wall thickness of pole at the bottom;
 DB = bolt diameter;
 E = Young's initial modulus of steel;
 E_t = tangential modulus;
 E_x = longitudinal elastic modulus;
 F_y = yield stress;
 G = shear modulus;
 L = pole length;
 LP = length of below top of pole;
 LS = length of steel anchor base;
 PD = side length/diameter of square/circular base plate;
 PT = thickness of base plate;
 TT = wall thickness of pole at top;
 v_f = fiber volume fraction;
 w_f = fiber weight fraction;
 ρ = density;
 σ_x = longitudinal tensile strength;
 ν = Poisson's ratio;
 μ = coefficient of friction; and
 δ_u = ratio of ultimate elongation (%).

References

- Abolmaali, A., Yuan, R. L., Choi, Y., and Shah, A. (2004). "Stiffness characteristics of closed-circuit television camera steel poles." *Proc., 84th Transportation Research Board Conf.*, Transportation Research Board, Washington, D.C.
- Bahaari, M. R., and Sherbourne, A. N. (2000). "Behavior of eight-bolt large capacity endplate connections." *Comput. Struct.*, 77, 315–325.
- Choi, C. K., and Chung, G. T. (1996). "A gap element for three-dimensional elastoplastic contact problems." *Comput. Struct.*, 61(6), 1155–1167.
- Chutima, S., and Blackie, A. P. (1996). "Effect of pitch distance, row spacing, end distance and bolt diameter on multifastened composite joints." *Composites, Part A*, 27(2), 105–110.
- Citipitioglu, A. M., Haj-Ali, R. M., and White, D. W. (2002). "Refined 3D finite element modeling of partially restrained connections including slip." *J. Constr. Steel Res.*, 58, 995–1013.
- Dicleli, M. (1997). "Computer-aided optimum design of steel tubular telescopic pole structures." *Comput. Struct.*, 62(6), 961–973.
- Fu, G., and Boulos, S. J. (1996). "Finite element analysis of irregular thick plates for signal pole design." *Comput. Struct.*, 58(1), 221–232.
- Ibrahim, S., and Polyzois, D. (1999). "Ovalization analysis of fiber-reinforced plastic poles." *Compos. Struct.*, 45, 7–12.
- Kishi, N., Ahmed, A., and Yabuki, N. (2001). "Nonlinear finite element analysis of top- and seat-angle with double web-angle connections." *Struct. Eng. Mech.*, 12(2) 201–214.
- Krishnamurthy, N. (1978). "Fresh look at bolted end-plate behavior and design." *Eng. J.*, (AISC), 15(2), 39–49.
- Kukreti, A. R., Ghassemieh, M., and Murray, T. M. (1990). "Behavior and design of large-capacity moment-endplates." *J. Struct. Eng.*, 116(3), 809–828.
- Kulak, G. L., and Birkemoe, P. C. (1993). "Field studies of bolt pretension." *J. Constr. Steel Res.*, 25, 95–106.
- Lacoursiere, B. (1999). "Steel utility poles: Advantages and application." IEEE Conf. Paper, No. B2.
- Lin, Z. M. (1995). "Analysis of pole-type structures of fibre-reinforced plastics by finite element method," Ph.D. dissertation, University of Manitoba, Canada.
- Polyzois, D., Ibrahim, S., and Raftoyiannis, I. G. (1999). "Performance of fiber-reinforced plastic tapered poles under lateral loading." *J. Compos. Mater.*, 33(10), 941–960.
- Polyzois, D., Raftoyiannis, I. G., and Ibrahim, S. (1998). "Finite elements method for the dynamic analysis of tapered composite poles." *Compos. Struct.*, 43, 25–34.
- Richard, R. M., and Abbott, B. J. (1975). "Versatile elastic-plastic stress-strain formula." *J. Eng. Mech. Div., Am. Soc. Civ. Eng.*, 101(EM4), 511–515.
- Stallings, J. M., and Hwang, D. Y. (1992). "Modeling pretensions in bolted connections." *Comput. Struct.*, 45(4), 801–803.
- Wanzek, T., and Gebbeken, N. (1999). "Numerical aspects for the simulation of end plate connections." *Virdi KS, Rep. of Working Group 6—Numerical simulation of semirigid connections by the finite element method*, Brussels, Luxembourg, 13–31.
- Yorgun, C., Dalci, S., and Altay, G. A. (2004). "Finite element modeling of bolted steel connections designed by double channel." *Comput. Struct.*, 82, 2563–2571.